J. Mech. Phys. Solids 99 (2017) 163–177

Contents lists available at ScienceDirect

Journal of the Mechanics and Physics of Solids

journal homepage: www.elsevier.com/locate/jmps

Interface elasticity effects in polymer-filled nanoporous metals

J. Wilmers[a,*], A. McBride[b,c], S. Bargmann[d]

[a] Institute of Materials Research, Helmholtz-Zentrum Geesthacht, Germany
[b] Division of Infrastructure and Environment, School of Engineering, The University of Glasgow, United Kingdom
[c] Centre for Research in Computational and Applied Mechanics, University of Cape Town, South Africa
[d] Institute of Continuum Mechanics and Material Mechanics, Hamburg University of Technology, Germany

ARTICLE INFO

Keywords:
Composite
Nanoporous
Multiphysics
Interface
Micromechanics

ABSTRACT

A continuum formulation for electroactive composites made from nanoporous gold and ion-conducting polymer is proposed. A novel extension of surface elasticity theory is developed to account for the high surface-to-volume ratio of nanoporous gold, and to capture the chemoelectromechanical coupling that occurs on the interface between the metal and the polymer. This continuum formulation accounts for the fully non-linear behaviour exhibited by the composite.

The balance of linear momentum, Gauß's flux theorem and a relation for the transport of charge carriers are introduced in the bulk material as well as on the interface to describe the non-linear multiphysics and highly coupled response of the actuator. The resulting system of non-linear equations is solved using the finite element method. A series of numerical examples is presented to elucidate the theory.

1. Introduction

Actuators translate electrical or chemical energy into mechanical work and are, therefore, crucial in a variety of technical applications, including robotics (Chi and Xu, 2014; McEvoy and Correll, 2015) or chemical engineering, e.g., in pumps (Laser and Santiago, 2004). In such applications, functional materials which exhibit a strong coupling between their mechanical and, e.g., magnetic or electric behaviour are utilised.

Electromechanical coupling, which allows for the translation of electric signals into deformation or vice versa, occurs in various materials and can be tailored to different applications (Wilson et al., 2007). For example, piezoceramics exhibit a fast response time, a high mechanical strength and very small strain amplitudes (Uchino, 1998). Electroactive polymers, by contrast, exhibit actuation strains in the region of 10% which are about two orders of magnitude larger than those in piezoceramics (Shahinpoor et al., 1998; Bar-Cohen, 2010). The large strains and the low voltages required for their operation have led to considerable interest in actuators, sensors and energy harvesters based on electroactive polymers in the last decade. There exist numerous different types of electroactive polymers that differ not only in properties such as actuation strain, operating voltages or their capacitance but also in the underlying coupling mechanisms.

These different actuation mechanisms produce a variety of possible responses and, therefore, require different modelling approaches. For instance, the active behaviour in so-called electronically activated polymers is based on piezoelectric or electrostrictive effects and is commonly modelled using the concept of the Maxwell stress to express the mechanical effect of electric forces, see, e.g., Hong (2011) and Bustamante and Rajagopal (2013).

Ionically activated polymers, on the other hand, require the investigation of ion transport coupled to the electrical and

* Corresponding author at: Institute of Materials Research, Helmholtz-Zentrum Geesthacht, Germany.

http://dx.doi.org/10.1016/j.jmps.2016.11.011
Received 3 December 2015; Received in revised form 6 September 2016; Accepted 17 November 2016
Available online 22 November 2016

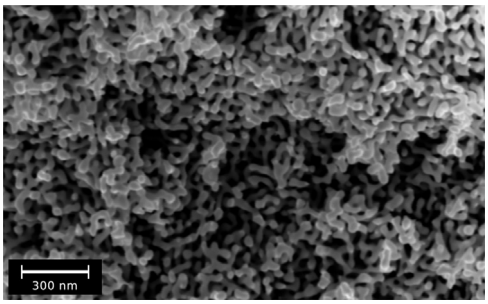

Fig. 1. Scanning electron micrograph of nanoporous gold showing the interconnected network of pores that is responsible for the exceptionally high surface-to-volume ratio. The gold nanowires have a diameter of ca. 30 nm. (Image courtesy of Nadiia Mameka at Helmholtz-Zentrum Geesthacht.)

mechanical behaviour of the material. The most prominent example of this class of electroactive polymers are ionic polymers (Jo et al., 2013). They are typically realised in composites of the hydrated polymer with metal electrodes, so called ionic polymer metal composites (IPMCs). Phenomenological modelling approaches often exploit the typical layered bending setup of IPMCs actuators (Alici et al., 2008; Fang et al., 2008; Mutlu et al., 2014) but neglect ion transport. To describe ion transport the Poisson-Nernst-Planck framework is most commonly used. In Porfiri (2008), an analytical solution for the Poisson-Nernst-Planck equations is presented. Nemat-Nasser and Li (2000); Pugal et al. (2011) and Nardinocchi et al. (2011) extend the Poisson-Nernst-Planck equations to account for chemoelectromechanical coupling in IPMC actuators. Such physics-based models provide valuable insight into the underlying mechanisms of, for example, actuation (Cha and Porfiri, 2014), back relaxation phenomena (Schicker and Wallmersperger, 2013) and sensing (Farinholt and Leo, 2004; Chen et al., 2007; Aureli and Porfiri, 2013; Cha et al., 2013) in IPMCs. Furthermore, these models introduce many concepts to describe the various types of electroactive polymers.

Another class of materials that has recently gained attention for its electromechanically coupled behaviour are nanoporous metals which have a unique structure of interconnected nanoscale wires, cf. Fig. 1, resulting in an expectationally high surface-to-volume ratio. Due to this high surface-to-volume ratio, seemingly small surface modifications strongly affect the mechanical behaviour. For example, if immersed in a liquid electrolyte, nanoporous metals exhibit macroscopic actuation behaviour, due to electrically charging the metal's surface and electroadsorption of a monolayer of ions (Weissmüller et al., 2003; Jin and Weissmüller, 2010). This charging induces variations of the surface stress that are visible in a deformation of the bulk material.

Furthermore, an electrostatic modification of the surface of nanoporous metals alters the metal's mechanical properties. For example, Mameka et al. (2014) conducted a compression test on a nanoporous gold sample during potential sweeps, showing that the material's stiffness is increased up to ~8% by surface modification. As surface modification is caused by interaction with charge carriers that migrate in an electric field, these effects are fully reversible by removing or reversing the applied electric potential.

To date, utilisation of electromechanical coupling in nanoporous metals requires an electrolyte to provide ions. As most common electrolytes are liquids, potential applications of nanoporus metal actuators are limited to environments in which evaporation of the electrolyte is prevented and contact with aqueous or flammable liquids is uncritical. However, recent studies aiming to overcome this limitation, propose nanocomposites of nanoporous metals and electroactive polymers (Lang et al., 2012). In the same vein, a completely dry setup in which the nanoporous metal is filled with a polymeric solid electrolyte is desirable.

Upon application of an electric potential, ions migrate within the polymer towards the metal/polymer interface. Just as in liquid electrolyte setups, ions interact with the metal surface and, thus, induce stresses and modify the interface. Consequently, the fundamental processes occurring in a dry setup are the same as in setups with liquid electrolytes. However, in solid electrolytes, ion transport takes place at different time scales and may be much slower or faster than the transport in liquid electrolytes depending on the material. Furthermore, regions of ion excess formed at the metal/polymer interface induce stresses within the polymer that result in macroscopic deformation (Shahinpoor et al., 1998; Mazzoldi et al., 1998) that is superimposed on the deformation of the metal. The behaviour in composite actuators, therefore, is considerably more complex and requires a new theoretical framework that is able to capture both bulk and interface mechanisms of electromechanical coupling.

In the following, such a material model for an electroactive metal/polymer composite that incorporates electromechanical coupling and focusses on the pronounced influence of the metal/polymer interface is introduced. To this end, an interface elasticity framework is combined with a continuum mechanical model that couples the mechanical behaviour of the metal and the polymer with ion transport in an electric field occurring in the polymer.

Classical continuum theories generally do not account for the influence surfaces and interfaces have on the response of the bulk material. Their role, however, becomes significant if one considers nanoporous materials which are characterised by a large surface-to-volume ratio. In the proposed model, the important impact of interfaces on the overall functionality of the actuator is described using an extension of the surface elasticity theory of Gurtin and Murdoch (1975). In this theory, surfaces are endowed with their own thermodynamic structure, that is, they have their own free energy and a resulting stress measure which is governed by a balance equation. The consistent micro-to-macro transition for Gurtin-Murdoch type interfaces is introduced in McBride et al. (2012).

In the following, the balance of linear momentum, Gauß's flux theorem and a relation for the transport of charge carriers are developed in the bulk and on the interface to describe the highly coupled response of the actuator. In addition, the continuum formulation accounts for the physically reasonable fully non-linear (geometric and material) response exhibited by electroactive composites.

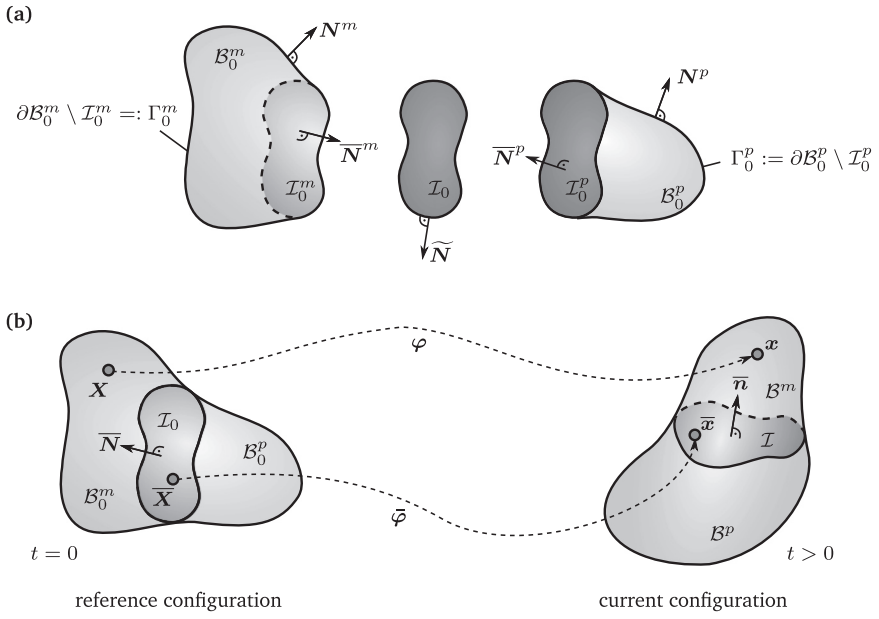

Fig. 2. Schematic representation of a continuum body $\mathcal{B}_0$ that is separated into two domains $\mathcal{B}_0^m$ and $\mathcal{B}_0^p$ by the coherent interface $\mathcal{I}_0$. (a) Each of the two volumes includes one side of the interface $\mathcal{I}_0$. For the corresponding interface normals the relation $\overline{\boldsymbol{N}}(\boldsymbol{X}) := \overline{\boldsymbol{N}}^p(\boldsymbol{X}) = -\overline{\boldsymbol{N}}^m(\boldsymbol{X})$ holds. (b) Material points are mapped from the reference configuration to the current configuration by the motions $\boldsymbol{\varphi}$ and $\overline{\boldsymbol{\varphi}} = \boldsymbol{\varphi}|_{\mathcal{I}_0}$.

2. Governing equations

A metal/ion-conducting polymer composite can be described as a body consisting of three physical domains that exhibit considerably different behaviour, namely the metal, the polymer, and the metal/polymer interface. In the model, the domains are represented in a decomposition of a continuum body $\mathcal{B}_0$ in the reference configuration according to $\mathcal{B}_0 = \mathcal{B}_0^m \cup \mathcal{I}_0 \cup \mathcal{B}_0^p$, see Fig. 2, where the disjoint union $\mathcal{B}_0 := \mathcal{B}_0^m \cup \mathcal{B}_0^p$ represents the bulk and $\mathcal{I}_0$ is the interface. The position of a material point in $\mathcal{B}_0$ is denoted by $\boldsymbol{X}$ and is mapped to the current configuration at time t via the motion $\boldsymbol{\varphi}$ as $\boldsymbol{x} = \boldsymbol{\varphi}(\boldsymbol{X}, t)$. The interface $\mathcal{I}_0$ is assumed to be material and geometrically coherent, i.e., there is no discontinuity in the motion $\boldsymbol{\varphi}$ over the interface and a material point on the interface is denoted by $\overline{\boldsymbol{X}} = \boldsymbol{X}|_{\mathcal{I}_0}$. Here and in the following, interface properties are denoted by an overbar $\overline{\bullet}$. Furthermore, no bulk material is transported over the interface, i.e., every material point $\boldsymbol{X}^m$, $\boldsymbol{X}^p$ and $\overline{\boldsymbol{X}}$ remains in its initial domain.

The deformation gradients in the bulk and on the interface are defined by

$$\boldsymbol{F} := \mathrm{Grad}\,\boldsymbol{\varphi} \quad \text{and} \quad \overline{\boldsymbol{F}} := \overline{\mathrm{Grad}}\,\overline{\boldsymbol{\varphi}},$$

where the interface gradient operator is the projection of the bulk operator to the interface $\overline{\mathrm{Grad}}\bullet := \mathrm{Grad}\bullet \cdot \overline{\boldsymbol{I}}$ with the rank-deficient second-order interface identity tensor $\overline{\boldsymbol{I}} := \boldsymbol{I} - \overline{\boldsymbol{N}} \otimes \overline{\boldsymbol{N}}$. The link to the notation adopted here and a representation in a curvilinear coordinate system is presented in Javili et al. (2014). The interface divergence is defined by $\overline{\mathrm{Div}}\bullet := \overline{\mathrm{Grad}}\bullet : \overline{\boldsymbol{I}}$. A jump of a quantity $\bullet$ over the interface $\mathcal{I}_0$ is defined by $[\![\bullet]\!] := \bullet|_{\mathcal{I}_0^m} - \bullet|_{\mathcal{I}_0^p}$, where $\mathcal{I}_0^m$ and $\mathcal{I}_0^p$ denote the two sides of the interface.

The extended divergence theorems in the bulk and on the interface are given by

$$\int_{\mathcal{B}_0} \mathrm{Div}(\bullet)\,\mathrm{d}V = \int_{\partial\mathcal{B}_0} \bullet \cdot \boldsymbol{N}\,\mathrm{d}A - \int_{\mathcal{I}_0} [\![\bullet]\!] \cdot \overline{\boldsymbol{N}}\,\mathrm{d}A, \tag{1a}$$

$$\int_{\mathcal{I}_0} \overline{\mathrm{Div}}(\overline{\bullet})\,\mathrm{d}V = \int_{\partial\mathcal{I}_0} \overline{\bullet} \cdot \widetilde{\boldsymbol{N}}\,\mathrm{d}L + \int_{\mathcal{I}_0} \overline{\mathrm{Div}}\,\overline{\boldsymbol{N}}\,\overline{\bullet} \cdot \overline{\boldsymbol{N}}\,\mathrm{d}A, \tag{1b}$$

where $\boldsymbol{N}$ and $\widetilde{\boldsymbol{N}}$ are the normal vectors to the body's surface and the curve bounding the interface, respectively. For further details, refer to Javili et al. (2013).

Using these definitions and identities, the governing equations for the primary fields, i.e., the displacement, electric potential and ion concentration, in the bulk and on the interface are derived from fundamental balance equations.

The proposed interface elasticity framework accounts for the unique behaviour of nanoporous metals (and other nanoscale materials) that arises due to the large surface-to-volume ratio these materials exhibit. Thus, seemingly small changes in the surface properties can have a noticeable influence on the overall material behaviour. For instance, the electroactive behaviour in nanoporous metals is a direct consequence of changes in the surface energy due to electroadsorption of electrolyte ions (Jin and Weissmüller, 2010). Such effects are naturally described in the proposed framework as it takes into account interface energies and interface properties.

Furthermore, the extention to include interphase effects in the proposed model is straight-forward. An alternative approach to

model interphases like those in ionomeric polymer/metal composites has been proposed by Cha et al. (2012). Here, interphases in which metal particles are dispersed in the polymer and which result from the composite production are modelled using the concept of composite layers, whereby interphases are homogenised to account for their distinct influence on the electrical properties of the composite. In the present contribution, however, the interface-enhanced framework is used to model effects that purely result from the physics of a polymer/metal interface exhibiting perfect contact.

2.1. Deformation

Following the presentation by Javili and Steinmann (2010) and extending it to account for inertia effects, the global balance of linear momentum for a continuum body $\mathcal{B}_0$ with a coherent interface $\mathcal{I}_0$ is derived from the integral balance:

$$\int_{\mathcal{B}_0} \rho_0 \ddot{\boldsymbol{u}} \mathrm{d}V + \int_{\mathcal{I}_0} \overline{\rho}_0 \ddot{\overline{\boldsymbol{u}}} \mathrm{d}A = \int_{\partial\mathcal{B}_0} \boldsymbol{P}\cdot\boldsymbol{N}\mathrm{d}A + \int_{\partial\mathcal{I}_0} \overline{\boldsymbol{P}}\cdot\overline{\boldsymbol{N}}\mathrm{d}L + \int_{\mathcal{B}_0} \boldsymbol{B}\mathrm{d}V + \int_{\mathcal{I}_0} \overline{\boldsymbol{B}}\mathrm{d}A. \tag{2}$$

Here, $\rho_0\left[\frac{kg}{m^3}\right]$ and $\overline{\rho}_0\left[\frac{kg}{m^2}\right]$ are the mass densities with respect to the reference bulk volume and reference interface area, respectively. The displacement vector is denoted by $\boldsymbol{u}$, $\boldsymbol{P}$ is the first Piola-Kirchhoff stress tensor and $\boldsymbol{B}$ and $\overline{\boldsymbol{B}}$ are body forces. A superimposed dot denotes a material time derivative. As every material point $\overline{\boldsymbol{X}}$ remains on the interface during deformation, time derivatives are well-defined on the interface. For details of the extension to a moving interface, refer to Cermelli et al. (2005).

As the interface is assumed to be mechanically coherent, there is no jump in the displacement over the interface and, hence, $\overline{\boldsymbol{u}} = \boldsymbol{u}|_{\mathcal{I}_0^p} = \boldsymbol{u}|_{\mathcal{I}_0^m}$.

Localising Eq. (2) for an arbitrary control region in the bulk that does not include any part of the interface yields the balance of linear momentum in the well known form

$$\rho_0 \ddot{\boldsymbol{u}} = \mathrm{Div}\,\boldsymbol{P} + \boldsymbol{B} \quad \text{in } \mathcal{B}_0. \tag{3}$$

At a point $\overline{\boldsymbol{X}} \in \mathcal{I}_0$, using the divergence theorems in the bulk Eq. (1a) and on the interface Eq. (1b) the balance of linear momentum becomes

$$\frac{\mathrm{d}}{\mathrm{d}t}\left[\int_{\mathcal{B}_0} \rho_0 \dot{\boldsymbol{u}}\mathrm{d}V + \int_{\mathcal{I}_0} \overline{\rho}_0 \dot{\overline{\boldsymbol{u}}}\mathrm{d}A\right] = \int_{\mathcal{B}_0} \mathrm{Div}\,\boldsymbol{P}\mathrm{d}V - \int_{\mathcal{I}_0} [\![\boldsymbol{P}]\!]\cdot\overline{\boldsymbol{N}}\mathrm{d}A + \int_{\mathcal{I}_0} \overline{\mathrm{Div}}\,\overline{\boldsymbol{P}}\mathrm{d}A + \int_{\partial\mathcal{I}_0} \overline{\mathrm{Div}}\,\overline{\boldsymbol{N}}\,[\overline{\boldsymbol{P}}\cdot\overline{\boldsymbol{N}}]\mathrm{d}L + \int_{\mathcal{B}_0} \boldsymbol{B}\mathrm{d}V + \int_{\mathcal{I}_0} \overline{\boldsymbol{B}}\mathrm{d}A. \tag{4}$$

Recognising that the interface Piola-Kirchhoff stress $\overline{\boldsymbol{P}}$ is, by definition, a superficial tensor and, therefore, $\overline{\boldsymbol{P}}\cdot\overline{\boldsymbol{N}} = 0$, localisation for $\mathcal{B}_0 \to \varnothing$ (resp. $\mathcal{B}_0 \to \mathcal{I}_0$) yields the balance of linear momentum for the interface

$$\overline{\rho}_0 \ddot{\overline{\boldsymbol{u}}} = \overline{\mathrm{Div}}\,\overline{\boldsymbol{P}} + \overline{\boldsymbol{B}} + [\![\boldsymbol{P}]\!]\cdot\overline{\boldsymbol{N}} \quad \text{on } \mathcal{I}_0. \tag{5}$$

Following a similar argument to Javili et al. (2013), the balance of angular momentum reduces to

$$\boldsymbol{F}\cdot\boldsymbol{P}^T = \boldsymbol{P}\cdot\boldsymbol{F}^T \quad \text{in } \mathcal{B}_0, \tag{6}$$

$$\overline{\boldsymbol{F}}\cdot\overline{\boldsymbol{P}}^T = \overline{\boldsymbol{P}}\cdot\overline{\boldsymbol{F}}^T \quad \text{on } \mathcal{I}_0. \tag{7}$$

2.2. Electrostatics

For ion-conducting polymers, any changes in the electric fields can be considered instantaneous in comparison to the slow charge carrier transport occurring in ion-conducting polymers (Hallinan and Balsara, 2013). Therefore, the evolution of electric fields upon application of an electric potential is described within the electrostatic framework. Furthermore, magnetic fields are not considered as their influence on ion transport is negligible.

In the electrostatic framework, the electric field with respect to the reference configuration,[1] i.e., the nominal electric field, is denoted by E and defines the electric potential by $\mathsf{E} =: -\mathrm{Grad}\,\Phi$.

The sources of electric fields are electric charge carriers which, in a continuum framework, can be described by "smeared" charge densities $q_0(\boldsymbol{X})$. In condensed matter, one can distinguish between mobile, "free", charges q_0^f such as electrons or ions, and bound charges q_0^b which arise from dipole moments in a polarisable material.

To separate the effects arising from the different kinds of charges, the nominal polarisation field $\mathsf{P}(\mathsf{E})$ describing the dipole density and the nominal electric displacement field $\mathsf{D}(\mathsf{E})$ are introduced (Dorfmann and Ogden, 2014). These three fields are related by

$$\mathsf{D} := \varepsilon_0 J\boldsymbol{C}^{-1}\cdot\mathsf{E} + \mathsf{P}, \tag{8}$$

where ε_0 is the vacuum permittivity, J is the determinant of the deformation gradient $\boldsymbol{F}$ and $\boldsymbol{C} = \boldsymbol{F}^T\cdot\boldsymbol{F}$ denotes the right Cauchy-

[1] Note that, classically, electrostatic fields and relations are defined in the current configuration. Details on the pull back employed here and in the following can be found in Dorfmann and Ogden (2005).

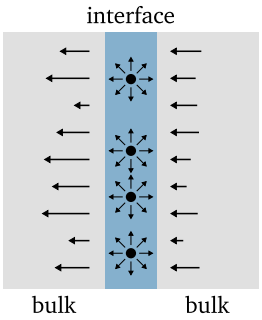

Fig. 3. Schematic representation of the electric field induced by (positive) interface charges.

Green deformation tensor.

Gauß's flux theorem relates the electric flux through a closed surface to the enclosed electric charges and follows from the time integration of the charge carrier mass balance. Following Chatzigeorgiou et al. (2014) (an electrostatics framework accounting for surface effects), Gauß's law for the bulk and the interface is given by

$$0 = -\int_{\partial\mathcal{B}_0} \mathsf{D}\cdot\boldsymbol{N}\,\mathrm{d}A - \int_{\partial\mathcal{I}_0} \overline{\mathsf{D}}\cdot\widetilde{\boldsymbol{N}}\,\mathrm{d}L + \int_{\mathcal{B}_0} q_0^f\,\mathrm{d}V + \int_{\mathcal{I}_0} \overline{q}_0^f\,\mathrm{d}A, \tag{9}$$

Here, the free charge density q_0^f is the sum over all free charges present and, thus, is expressed in terms of the concentrations of the different charge carrier types c_0^i as $q_0^f(\boldsymbol{X}) = F\sum_i z^i c_0^i(\boldsymbol{X})$ with the Faraday constant F and the species valence z^i.

Localisation of Eq. (9) using the same arguments as employed for the linear momentum balance in Section 2.1, and applying the divergence theorems for the bulk Eq. (1a) and the interface Eq. (1b), yields

$$0 = -\mathrm{Div}\,\mathsf{D} + q_0^f \quad \text{in } \mathcal{B}_0, \tag{10}$$

$$0 = -\overline{\mathrm{Div}}\,\overline{\mathsf{D}} + \overline{\mathrm{Div}}\,\overline{\boldsymbol{N}}\,[\overline{\mathsf{D}}\cdot\overline{\boldsymbol{N}}] + \overline{q}_0^f - [\![\mathsf{D}\cdot\overline{\boldsymbol{N}}\quad \text{on } \mathcal{I}_0. \tag{11}$$

As the electric displacement field originates from free charges that emit fields in all directions (see Fig. 3), $\overline{\mathsf{D}}$ is, unlike the interface fields introduced in Sections 2.1 and 2.3, not a tangential vector. Thus, the second right-hand-side term of Eq. (11) does not vanish as it does in the other interface equations.

2.3. Charge carrier transport

Charge carriers are transported within a body as a reaction to an applied electric field. To describe this transport, the balance of mobile species mass is evaluated as the charge carrier mass is a conserved quantity. The relations derived in the following are valid for any mass transport phenomenon, such as diffusion or advection. To maintain this generality, no assumptions about the continuity of material fluxes or concentrations over the boundary $\mathcal{I}_0$ are made.

The mass balance for the diffusing species i is expressed in terms of the mass concentration in the bulk c_0^i [mol/m^3] and on the interface $\overline{c}_0^i$ [mol/m^2]. The concentration is given as the amount of ions per volume or area, respectively, with respect to the reference configuration. This yields the mass balance for the system

$$\int_{\mathcal{B}_0} \dot{c}_0^i\,\mathrm{d}V + \int_{\mathcal{I}_0} \dot{\overline{c}}_0^i\,\mathrm{d}A = -\int_{\partial\mathcal{B}_0} \boldsymbol{J}^i\cdot\boldsymbol{N}\,\mathrm{d}A - \int_{\partial\mathcal{I}_0} \overline{\boldsymbol{J}}^i\cdot\widetilde{\boldsymbol{N}}\,\mathrm{d}L + \int_{\mathcal{B}_0} W^i\,\mathrm{d}V + \int_{\mathcal{I}_0} \overline{W}^i\,\mathrm{d}A. \tag{12}$$

The interface flux $\overline{\boldsymbol{J}}^i$ is a tangential vector that possesses the orthogonality property $\overline{\boldsymbol{J}}^i\cdot\overline{\boldsymbol{N}} = 0$. W^i and $\overline{W}^i$ are source terms that account for, e.g., chemical reactions that add or remove ions from the system. In most applications, these source terms vanish but they are included here for the sake of completeness.

Application of the divergence (Theorems (1a) and 1b) yields

$$\int_{\mathcal{B}_0} \dot{c}_0^i\,\mathrm{d}V + \int_{\mathcal{I}_0} \dot{\overline{c}}_0^i\,\mathrm{d}A = -\int_{\mathcal{B}_0} \mathrm{Div}\,\boldsymbol{J}^i\,\mathrm{d}V - \int_{\mathcal{I}_0} [\![\boldsymbol{J}^i]\!]\cdot\overline{\boldsymbol{N}}\,\mathrm{d}A - \int_{\mathcal{I}_0} \overline{\mathrm{Div}}\,\overline{\boldsymbol{J}}^i\,\mathrm{d}A + \int_{\mathcal{B}_0} W^i\,\mathrm{d}V + \int_{\mathcal{I}_0} \overline{W}^i\,\mathrm{d}A. \tag{13}$$

Localisation of Eq. (13) to the bulk and to the interface yields, for every diffusing species i, the general diffusion laws

$$\dot{c}_0^i = -\mathrm{Div}\,\boldsymbol{J}^i + W^i \quad \text{in } \mathcal{B}_0, \tag{14}$$

$$\dot{\overline{c}}_0^i = -\overline{\mathrm{Div}}\,\overline{\boldsymbol{J}}^i + \overline{W}^i - [\![\boldsymbol{J}^i]\!]\cdot\overline{\boldsymbol{N}} \quad \text{on } \mathcal{I}_0. \tag{15}$$

Similarly, diffusion laws with respect to an energetic surface are presented in McBride et al. (2011).

The balance equations on the interface are valid for any mass transport mechanism. The nature of the transport is described by the constitutive relations for the diffusion fluxes $\boldsymbol{J}^i$ and $\overline{\boldsymbol{J}}^i$. Furthermore, the behaviour at the interface has to be specified for different transport phenomena.

For the limiting case of a non-permeable interface, such as the one in a metal/ion-conducting polymer composite, $\boldsymbol{J}^i\cdot\overline{\boldsymbol{N}} = 0$ and,

thus, any change in the interface concentration solely arises from interface effects according to $\dot{\overline{c}}_0^i = -\overline{\mathrm{Div}}\,\overline{\boldsymbol{J}}^i + \overline{W}^i$.

Assuming continuity in the concentration over the interface, i.e., $[\![c_0^i]\!] = 0$, the interface concentration becomes $\overline{c}_0^i = c_0^i|_{I_0^m} = c_0^i|_{I_0^p} = c_0^i|_{I_0}$. This case could be called a "highly diffusive" interface following the terminology for heat conduction across interfaces, see Javili et al. (2013).

2.4. Balances of energy and entropy

Transport of ions within the polymer network is associated with the "mixing" of ions and polymer chains. This mixing contributes to the system's internal energy and entropy via the specific enthalpy φ^{mix^i} and the specific entropy η^{mix^i}. These two quantities define the chemical potential of mixing $\mu^{\mathrm{mix}^i} := \varphi^{\mathrm{mix}^i} - \theta\eta^{\mathrm{mix}^i}$, where θ is the absolute temperature.

Furthermore, the charge carried by the ions contributes to the system's energy. In an electrostatic framework, the potential energy per charge is described by the electric potential Φ. Thus, the balance of internal energy for the system includes mechanical, electrical and chemical contributions and is given by:

$$\rho_0\dot{e} = \boldsymbol{P}\colon\dot{\boldsymbol{F}} - \dot{\mathsf{D}}\cdot\mathrm{Grad}\,\Phi - \sum_i [\Phi F z^i c_0^i - \varphi^{\mathrm{mix}^i}\dot{c}_0^i + \boldsymbol{J}^i\cdot\mathrm{Grad}\,\varphi^{\mathrm{mix}^i}] \quad \text{in } \mathcal{B}_0, \tag{16}$$

$$\overline{\rho}_0\dot{\overline{e}} = \overline{\boldsymbol{P}}\colon\dot{\overline{\boldsymbol{F}}} - \dot{\overline{\Phi}}F\sum_i z^i\dot{\overline{c}}_0^i - \dot{\overline{\mathsf{D}}}\cdot\overline{\mathrm{Grad}}\,\overline{\Phi} + \sum_i [\overline{\varphi}^{\mathrm{mix}^i}\dot{\overline{c}}_0^i - \overline{\boldsymbol{J}}^i\cdot\overline{\mathrm{Grad}}\,\overline{\varphi}^{\mathrm{mix}^i} - [\varphi^{\mathrm{mix}^i} - \overline{\varphi}^{\mathrm{mix}^i}][\![\boldsymbol{J}^i\cdot\boldsymbol{N}]\!] \quad \text{on } \mathcal{I}_0. \tag{17}$$

Furthermore, the localised form of the entropy inequality reads

$$\rho_0\dot{\eta} - \sum_i [\eta^{\mathrm{mix}^i} - \boldsymbol{J}^i\cdot\mathrm{Grad}\,\eta^{\mathrm{mix}^i}] \geq 0 \quad \text{in } \mathcal{B}_0, \tag{18}$$

$$\overline{\rho}_0\dot{\overline{\eta}} - \sum_i [\overline{\eta}^{\mathrm{mix}^i} - \overline{\boldsymbol{J}}^i\cdot\overline{\mathrm{Grad}}\,\overline{\eta}^{\mathrm{mix}^i}] \geq 0 \quad \text{on } \mathcal{I}_0. \tag{19}$$

The full integral formulations of the balances of energy and entropy are presented in Appendix Appendix A. The isothermal case is considered here but it can easily be extended to account for thermal effects using the well-known principles of thermoelasticity.

Substituting the balances of internal energy into the entropy inequalities and evaluating them using the Coleman-Noll formalism yields the constitutive relations

$$\boldsymbol{P} = \rho_0\frac{\partial\Psi}{\partial\boldsymbol{F}} = 2\rho_0\boldsymbol{F}\cdot\frac{\partial\Psi}{\partial\boldsymbol{C}}, \quad \overline{\boldsymbol{P}} = \overline{\rho}_0\frac{\partial\overline{\Psi}}{\partial\overline{\boldsymbol{F}}} = 2\overline{\rho}_0\overline{\boldsymbol{F}}\frac{\partial\overline{\Psi}}{\partial\overline{\boldsymbol{C}}}, \; \mathsf{E} = \rho_0\frac{\partial\Psi}{\partial\mathsf{D}}, \quad \overline{\mathsf{E}} = \overline{\rho}_0\frac{\partial\overline{\Psi}}{\partial\overline{\mathsf{D}}}, \; \mu^{\mathrm{mix}^i} = Fz^i\Phi + \rho_0\frac{\partial\Psi}{\partial c_0^i}, \quad \overline{\mu}^{\mathrm{mix}^i} = Fz^i\overline{\Phi} + \overline{\rho}_0\frac{\partial\overline{\Psi}}{\partial\overline{c}_0^i},$$

as well as the requirements that

$$-\sum_i \boldsymbol{J}^i\cdot\mathrm{Grad}\,\mu^{\mathrm{mix}^i} \geq 0 \quad \text{and} \quad -\sum_i [\overline{\boldsymbol{J}}^i\cdot\overline{\mathrm{Grad}}\,\overline{\mu}^{\mathrm{mix}^i} + [\mu^{\mathrm{mix}^i} - \overline{\mu}^{\mathrm{mix}^i}][\![\boldsymbol{J}^i]\!]\cdot\boldsymbol{N}] \geq 0. \tag{20}$$

For the bulk, these relations are identical to ones for other types of electroactive polymers, e.g., Hong et al. (2010); Cha and Porfiri (2014).

3. Material modelling

The governing equations derived in Section 2 are summarised in Table 1. In order to model the behaviour of a metal/ion-conducting polymer composite, these equations are combined with appropriate constitutive equations that describe the different types of material behaviour observed in the ion-conducting polymer, in the metal and on the interface.

3.1. Ion-conducting polymer

In ion-conducting polymers, the conduction mechanism is based on transport of ions that are either introduced into the solid polymer bulk by doping or by immersion in a liquid electrolyte (Hallinan and Balsara, 2013). Migration of ions in an applied electric field leads to the build-up of space charges, i.e., ion accumulation in some areas and other areas that are ion-deprived. This causes deformation and stressing within the material, i.e., a chemoelectromechanical coupling in the bulk polymer. Polarisation of the polymer may induce stresses in the bulk as well. Furthermore, ions that are brought into contact with the electrode in this process

Table 1
Governing equations.

	Bulk	Interface
Linear momentum	$\rho_0\ddot{\boldsymbol{u}} = \mathrm{Div}\,\boldsymbol{P} + \boldsymbol{B}$	$\overline{\rho}_0\ddot{\overline{\boldsymbol{u}}} = \overline{\mathrm{Div}}\,\overline{\boldsymbol{P}} \quad + \overline{\boldsymbol{B}} + [\![\boldsymbol{P}]\!]\cdot\boldsymbol{N}$
Gauß's law	$0 = -\mathrm{Div}\,\mathsf{D} + q_0^f$	$0 = -\overline{\mathrm{Div}}\,\overline{\mathsf{D}} + \overline{\mathrm{Div}}\,\overline{\boldsymbol{N}}\,[\![\mathsf{D}\cdot\boldsymbol{N}]\!] + \overline{q}_0^f - [\![\mathsf{D}\cdot\boldsymbol{N}$
Diffusion	$\dot{c}_0 = -\mathrm{Div}\,\boldsymbol{J} + W$	$\dot{\overline{c}}_0 = -\overline{\mathrm{Div}}\,\overline{\boldsymbol{J}} \quad + \overline{W} - [\![\boldsymbol{J}]\!]\cdot\boldsymbol{N}$

are electroadsorbed onto the metal and, thus, alter the interface properties. These three mechanisms of electromechanical coupling are incorporated in the proposed model, where electroadsorption is captured by the interface model.

The behaviour of the bulk polymer is described by a Helmholtz free energy which is assumed to be additively decomposed into a part describing the purely mechanical behaviour and two parts describing the electrically and chemically induced behaviour:

$$\Psi(\boldsymbol{C}, \mathsf{D}, c_0) = \Psi^{\text{mech}}(\boldsymbol{C}) + \Psi^{\text{elecmech}}(\boldsymbol{C}, \mathsf{D}) + \Psi^{\text{chemmech}}(\boldsymbol{C}, c_0). \tag{21}$$

The purely mechanical part of the Helmholtz free energy is modelled by a Neo-Hookean material model:

$$\rho_0 \Psi^{\text{mech}}(\boldsymbol{C}) = \frac{\mu}{2}[\boldsymbol{C} - \boldsymbol{I}]\colon \boldsymbol{I} + \frac{\lambda}{2}\ln^2 J - \mu \ln J, \tag{22}$$

where μ and λ are the Lamé parameters. The electromechanical part of the free energy for an isotropic and electrically linear material is, following Cha and Porfiri (2014), given by

$$\rho_0 \Psi^{\text{elecmech}}(\boldsymbol{C}, \mathsf{D}) = \frac{1}{2\varepsilon_r \varepsilon_0}\frac{\boldsymbol{C}\colon \mathsf{D} \otimes \mathsf{D}}{J}. \tag{23}$$

The chemomechanical part of the Helmholtz free energy density is comprised of two contributions, the energy associated with deformation of the polymer in regions of ion excess or depletion and the energy of mixing these ions into the polymer network:

$$\rho_0 \Psi^{\text{chemmech}}(\boldsymbol{C}, c_0^{\text{mobile}}) = -\frac{1}{z^{\text{mobile}}} k q_0^f \ln J + R\theta\left[\ln\left(\frac{c_0^{\text{mobile}}}{c_0^{\text{initial}}}\right) - 1\right] c_0^{\text{mobile}}. \tag{24}$$

Here, the first term on the right-hand-side accounts for the coupling of concentration and deformation with the proportionality constant k. The second right-hand-side term is a classical expression for the mixing contribution, where R is the gas constant and c_0^{initial} denotes the mobile ion concentration in the initial state without any loads or potential differences applied. In the case of a single-ion conducting electrolyte as considered here, the free charge density is determined by $q_0^f = F[z^{\text{mobile}} c_0^{\text{mobile}} + z^{\text{immobile}} c_0^{\text{immobile}}]$.

Given this form of the Helmholtz free energy,[2] the first Piola-Kirchhoff stress tensor $\boldsymbol{P}$ in the polymer bulk is decomposed into a mechanically, an electromechanically and a chemomechanically induced contribution:

$$\begin{aligned}\boldsymbol{P} &= 2\boldsymbol{F}\cdot\frac{\partial \rho_0 \Psi}{\partial \boldsymbol{C}} = \mu \boldsymbol{F} + [\lambda \ln J - \mu]\boldsymbol{F}^{-T} - \frac{1}{J\varepsilon_r\varepsilon_0}\left[\frac{[\boldsymbol{C}\colon \mathsf{D} \otimes \mathsf{D}]}{2}\cdot\boldsymbol{F}^{-T} - \boldsymbol{F}\cdot\mathsf{D} \otimes \mathsf{D}\right] - \frac{1}{z^{\text{mobile}}} k q_0^f \boldsymbol{F}^{-T} \\ &= \boldsymbol{P}^{\text{mech}} + \boldsymbol{P}^{\text{elecmech}} + \boldsymbol{P}^{\text{chemmech}}.\end{aligned} \tag{25}$$

The electromechanical stress $\boldsymbol{P}^{\text{elecmech}}$ is the nominal Maxwell stress well known from the description of dielectric materials (see, e.g., Dorfmann and Ogden (2005); Ericksen (2007)). This stress contribution arises from forces induced during polarisation of the material in an electric field. The chemomechanical stress $\boldsymbol{P}^{\text{chemmech}}$, on the other hand, is caused by the free charge carrier accumulation and is proportional to the charge density. This relation is an extension of the one proposed in Nemat-Nasser and Li (2000) that also accounts for the mobile species valance z^{mobile} such that the stress is independent of the kind of mobile ion species and, thus, valid for various types of ion-conducting polymers. This coupling solely arises from stresses induced by the repulsive forces and molecular interactions in regions of high or low mobile charge carrier concentration. From here on, the superscript mobile will be omitted for readability.

The polymer has an isotropic and linear electric behaviour, so that

$$\mathsf{E} = \frac{\partial \rho_0 \Psi}{\partial \mathsf{D}} = \frac{1}{J\varepsilon_r\varepsilon_0}\boldsymbol{C}\cdot\mathsf{D}. \tag{26}$$

Recalling that the electric potential Φ is defined by $\mathsf{E} = -\text{Grad}\,\Phi$, Eq. (10) is written as

$$0 = \text{Div}(\varepsilon_0 \varepsilon_r J \boldsymbol{C}^{-1}\cdot\text{Grad}\,\Phi) + q_0^f.$$

The chemical potential of mixing is given by

$$\mu_s = \Phi F z + \frac{\partial \rho_0 \Psi}{\partial c_0} = F z[\Phi - k \ln J] + R\theta \ln\left(\frac{c_0}{c_0^{\text{initial}}}\right). \tag{27}$$

In combination with the requirement $-\boldsymbol{J}\cdot\text{Grad}\,\mu^{\text{mix}} \geq 0$, the constitutive expression for the ion flux can be determined. Transport of the free charge carriers is driven by the potential gradient and is also influenced by concentration gradients. Thus, the flux $\boldsymbol{J}$ of charge carrier species i can be described by a general relation $\boldsymbol{J} = -\boldsymbol{M}(\boldsymbol{C}, \Phi, c_0)\cdot\text{Grad}\,\mu^{\text{mix}}$, where $\boldsymbol{M}$ is the mobility tensor. With $\boldsymbol{M} = \frac{c_0}{R\theta}\boldsymbol{D}(c_0)$ and neglecting any dependence on the deformation state, this yields the classic Nernst-Planck equation as the sum of the fluxes arising from diffusion and migration as

[2] Note that this formulation for the Helmholtz free energy is limited to the most fundamental coupling and mixing effects, as the focus of this contribution is the development and presentation of a model accounting for interface effects in chemoelectromechanical coupling. Different choices for the Helmholtz free energy are possible, for example ones that take size effects into account, see, e.g., Borukhov et al. (2000) and Kilic et al. (2007).

$$\boldsymbol{J} = -\boldsymbol{D}\cdot\mathrm{Grad}\, c_0 + c_0\frac{zF}{R\theta}\boldsymbol{D}\cdot\boldsymbol{E} \quad \boldsymbol{J}^{\mathrm{diffusion}} + \boldsymbol{J}^{\mathrm{migration}}. \tag{28}$$

This formulation is valid for any transport mechanism, such as diffusion of solvated ions in a liquid or conformational movement of polymer chains.

Eq. (14) has to be solved for every free charge carrier species occurring in the material, which due to the requirement that charges are balanced within a body, are at least two. Here, a polymer electrolyte is considered in which either anions or cations are immobilised due to strong interactions with the polymer and only the counterions are free to move (Hallinan and Balsara, 2013). Taking into account that no ions are produced or destroyed within the material, yields the diffusion law

$$\dot{c}_0 = \mathrm{Div}(\boldsymbol{D}\cdot\mathrm{Grad}\, c_0) + \frac{zF}{R\theta}\mathrm{Div}(c_0\boldsymbol{D}\cdot\mathrm{Grad}\,\Phi) \tag{29}$$

for the mobile ions and a constant, homogeneous concentration distribution for the immobilised ions.

3.2. Metal

In a bulk metal, the charge carrier and electric potential distributions are assumed to be perfectly homogeneous for all phenomena occurring in this application case. Any charge building up in the metal is strictly localised to the interface and is, therefore, described by the interface formulation presented in Section 3.3. Hence, no further information would be gained from modelling electrostatics or ion transport within the metal bulk. Therefore, the modelling of the metal domain is limited to solving the non-linear momentum balance Eq. (6) together with a Neo-Hookean constitutive relation

$$\rho_0\Psi(\boldsymbol{C}) = \frac{\mu}{2}[\boldsymbol{C} - \boldsymbol{I}]\colon\boldsymbol{I} + \frac{\lambda}{2}\ln^2 J - \mu\ln J. \tag{30}$$

Thus, the first Piola-Kirchhoff stress is given by

$$\boldsymbol{P} = 2\boldsymbol{F}\cdot\frac{\partial\rho_0\Psi}{\partial\boldsymbol{C}} = \mu\boldsymbol{F} + [\lambda\ln J - \mu]\boldsymbol{F}^{-T}. \tag{31}$$

The metal considered here is gold, which, despite being a very exclusive material, is of great interest in case of nanoporous metals because under compression it deforms up to large plastic strains (e.g., up to 120% true strain (Wang and Weissmüller, 2013)), whereas nanomaterials usually only allow for small deformations. Current research aims at finding suitable materials that can replace gold and, thus, make electroactive nanocomposites available for diverse technical applications.

3.3. Interface

As both bulk materials exhibit a Neo-Hookean mechanical behaviour, the interface between them does as well. To account for the interface modification that occurs due to either capacitive charging or ion adsorption on the interface, a Helmholtz free energy has to be formulated that depends on the charge density at the interface $\overline{q}_0^f$. For nanoporous gold immersed in a liquid electrolyte, Mameka et al. (2014) investigated the electro-elastic coupling parameter $\bar{\xi}$ as the derivative of the surface elastic excess constant with respect to the surface charge density. Extending this definition to the interface Helmholtz energy in our model yields the definition

$$\bar{\xi}\overline{\boldsymbol{I}} := -\frac{\partial^3\overline{\rho}_0\overline{\Psi}}{\partial\overline{\boldsymbol{F}}^2\partial\overline{q}_0^f}, \tag{32}$$

with $\overline{\boldsymbol{I}}$ being the fourth-order interface identity tensor. With this, the electromechanically coupled interface Helmholtz free energy is expressed as

$$\overline{\rho}_0\overline{\Psi}(\overline{\boldsymbol{F}}, \overline{q}_0^f) = \frac{\overline{\mu}}{2}[\overline{\boldsymbol{F}}\colon\overline{\boldsymbol{F}} - 2] + \frac{\overline{\lambda}}{2}\ln^2\overline{J} - \overline{\mu}\ln\overline{J} - \frac{1}{2}\bar{\xi}\overline{q}_0^f\overline{\boldsymbol{F}}\colon\overline{\boldsymbol{F}}. \tag{33}$$

Electromechanical coupling at the interface arises from two different mechanisms that are connected to the two different kinds of charge carriers. There is electroadsorption in which ions are adsorbed onto the boundary and the formation of an interface charge which balances the space charge in the polymer by a shift of the electron concentration at the interface, see Fig. 4.

During electroadsorption, the monolayer of ions directly located at the polymer side of the interface $\overline{q}_0^f = q_0^f|_{I_0^p}$ is chemically adsorbed to the electrode and, thus, alters the interface stress. To describe this process, it is necessary to transfer the bulk concentration information to the interface using the relation $\bar{c}_0 = c_0\frac{V}{A}$, where A denotes the reference interface area and V the reference polymer volume.

The build-up of an interface charge in response to an applied electric field in a metallic conductor is described by the interface electrostatic Eq. (11). Furthermore, the classic interface condition for electric fields $\overline{\boldsymbol{N}}\times[\![\boldsymbol{E}]\!] = 0$ holds (see also Chatzigeorgiou et al. (2014)), i.e., the tangential component of the electric field is continuous across the interface. In a metallic conductor $\boldsymbol{E} = 0$, thus, it follows that the electric potential distribution is perfectly homogeneous along the interface (in fact, in the subsequent numerical implementation the electric potential is applied as a boundary condition on the interface). Hence, no separate interface effects occur and Eq. (11) on the interface reduces to

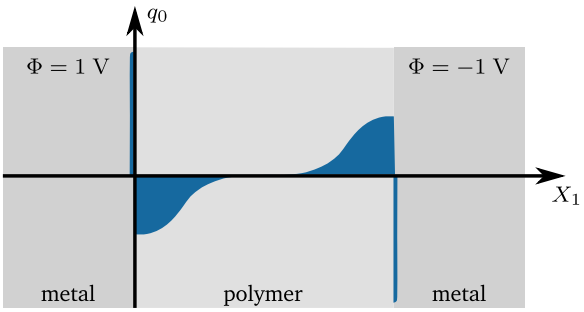

Fig. 4. Schematic depiction of the charge density distribution in an electrochemical cell consisting of two metal electrodes with an ion-conducting polymer electrolyte sandwiched in between. In the polymer, ions accumulate in a broad area at the metal/polymer interface. This charge accumulation induces a balancing charge in the metal surface by causing an increased or decreased electron concentration. Both kinds of charge are involved in the electromechanical coupling.

$$0 = \overline{q}_0^f - [\![\mathrm{D}]\!]\cdot\overline{\boldsymbol{N}}. \tag{34}$$

With this, the electromechanically coupled interface Helmholtz free energy is expressed as

$$\overline{\rho}_0\overline{\Psi}(\overline{\boldsymbol{F}}, \overline{q}_0^f) = \frac{1}{2}\overline{\lambda}\ln^2\overline{J} + \frac{1}{2}\overline{\mu}[\overline{\boldsymbol{F}}\colon\overline{\boldsymbol{F}} - 2 - 2\ln\overline{J}] - \frac{1}{2}\overline{\xi}\overline{q}_0^f\overline{\boldsymbol{F}}\colon\overline{\boldsymbol{F}} + R\overline{\theta}\left[\ln\left(\frac{\overline{c}_0}{\overline{c}_0^{\text{initial}}}\right) - 1\right]\overline{c}_0, \tag{35}$$

yielding an interface stress

$$\overline{\boldsymbol{P}} = \overline{\mu}\overline{\boldsymbol{F}} + [\overline{\lambda}\ln\overline{J} - \overline{\mu}]\overline{\boldsymbol{F}}^{-T} - \overline{\xi}\overline{q}_0^f\overline{\boldsymbol{F}}. \tag{36}$$

The mechanical interface parameters can be determined from density functional theory (Elsner et al.,) or molecular dynamics computations, while the coupling parameters $\overline{\xi}$ are identified from experiments (Mameka et al., 2014).

The charge carriers in a metal are electrons. Their transport along the interface is described by Eq. (15) which requires a constitutive expression for the diffusion flux $\overline{\boldsymbol{J}}$ that obeys the requirement Eq. (20)). Here, a non-permeable interface is considered, so that $[\![\boldsymbol{J}]\!]\cdot\overline{\boldsymbol{N}} = 0$. Hence, Eq. (20)) reduces to $-\overline{\boldsymbol{J}}\cdot\overline{\mathrm{Grad}}\,\overline{\mu}^{\mathrm{mix}} \geq 0$. This is fulfilled if $\overline{\boldsymbol{J}} = -\overline{\boldsymbol{M}}(\boldsymbol{C}, c_0^{\mathrm{el}})\cdot\overline{\mathrm{Grad}}\,\overline{\mu}^{\mathrm{mix}}$. With $\overline{\boldsymbol{D}} = R\overline{\theta}\frac{1}{\overline{c}_0^{\mathrm{el}}}\overline{\boldsymbol{M}}$ and the chemical potential

$$\overline{\mu}^{\mathrm{mix}} = Fz^{\mathrm{el}}\overline{\Phi} + \overline{\rho}_0\frac{\partial\overline{\Psi}}{\partial\overline{c}_0^{\mathrm{el}}} = Fz\overline{\Phi} + R\overline{\theta}\ln\left(\frac{\overline{c}_0^{\mathrm{el}}}{\overline{c}_0^{\mathrm{el,initial}}}\right), \tag{37}$$

this yields the expression

$$\overline{\boldsymbol{J}} = -\overline{\boldsymbol{D}}\cdot\overline{\mathrm{Grad}}\,\overline{c}_0^{\mathrm{el}}, \tag{38}$$

and the diffusion law

$$\dot{\overline{c}}_0^{\mathrm{el}} = \overline{\mathrm{Div}}(\overline{\boldsymbol{D}}\cdot\overline{\mathrm{Grad}}\,\overline{c}_0^{\mathrm{el}}). \tag{39}$$

4. Numerical example

In the following section, a structure consisting of a dry, single-ion-conducting polymer sandwiched inbetween two gold electrodes is considered as a benchmark example for a nanoporous metal/polymer composite to elucidate the theory developed in the previous sections. This sandwich structure is rigidly clamped on the bottom face and a potential difference of 1 V is applied as a boundary condition on the electrode surfaces, see Fig. 4. This setup highlights the different coupling mechanisms by having two differently charged interfaces. The material parameters used for the bulk and the interface are summarised in Tables 2 and 3, respectively.

4.1. Implementation

To solve the highly non-linear and strongly coupled system of equations, the finite element method is applied within an in-house code using the finite element library deal.II (Bangerth et al., 2007). Temporal discretisation is performed using a backward Euler finite difference scheme. An iterative Newton scheme is used to linearise and solve the resulting residual equations.

The interface is represented by a two-dimensional manifold that is embedded in the surrounding three-dimensional volume. The nodes of the interface mesh coincide with the respective nodes of the bulk mesh, thus, ensuring geometrical coherency in the solution. The deal.II library provides a number of routines and methods which calculate derivatives of fields on manifolds, thus, enabling a straightforward implementation of the interface operators.

This implementation is an extension of the surface-elasticity framework presented in Javili et al. (2014) and McBride et al. (2015) to interfaces (see also Davydov et al. (2014)). However, these frameworks deal with uncoupled mechanics problems only, i.e.,

Table 2
Bulk material parameters and constants.

	Symbol	Value	Source
Faraday constant	F	96485.337 C/mol	
Vacuum permittivity	ε_0	$8.854 \cdot 10^{-12}$ F/m	
Polymer			
Mass density	ρ_0	1.47 g/cm^3	Lòpez Cascales and Otero (2004)
Lamé parameters	λ	1.13 GPa	Vernitskaya and Efimov (1997)
	μ	0.75 GPa	
Relative permittivity	ε_r	$1 \cdot 10^3$	Aureli et al. (2009)
Valence mobile species	z	−1	
Mobile ion concentration	c_0	1200 mol/m^3	Pugal et al. (2012)
Diffusivity	D	$10 \cdot 10^{-11}$ m^2/s	Pugal et al. (2012)
Electromechanical coupling parameter	k	50 J/C	Nemat-Nasser and Li (2000)
Gold			
Mass density	ρ_0	19.3 g/cm^3	
Lamé parameters	λ	198.6 GPa	Balk et al. (2009)
	μ	27.08GPa	

the only degrees of freedom considered are the displacement components, which are continuous over the interface due to material and geometrical coherency. The metal/polymer composite modelled here exhibits electromechanical coupling and, thus, the framework is extended to a multiphysical one including electric potential and charge carrier concentration fields.

Furthermore, these fields differ between the three domains metal, polymer and interface. In the bulk metal, no electric fields or differences in the electron concentration occur, while both the interface and the polymer require information about the electric potential and, respectively, the electron and ion concentration.

In addition, special care has to be taken in mapping information from the bulk to the interface because the interface equations are coupled to bulk values, for example in the jumps of fields over the interface or in determining the ion concentration at the interface.

4.2. Boundary conditions

The response of the sandwich structure presented in Fig. 5 to an applied potential difference is modelled here. The specimen's bottom face is mechanically constrained in all directions and a potential difference of 1 V is applied using constant Dirichlet boundary conditions imposed on the nodes located at the metal/polymer interface. This choice of the boundary conditions takes into account that the electric potential in a perfect conductor such as gold is homogeneous and models a potential difference that is held constant after application, i.e., a voltage step load.

The ion flux is assumed to be zero over all surfaces, i.e., no charge carriers can leave the volume. Furthermore, the interface between polymer and metal is modelled as non-permeable, that is $\boldsymbol{J} \cdot \overline{\boldsymbol{N}} = 0$, because ions cannot cross the interface to enter the metal. The displacement and the electric potential on the other hand are assumed to be continuous over the interface, i.e., $\overline{\boldsymbol{u}} = \boldsymbol{u}|_{I_0}$ and $\overline{\Phi} = \Phi|_{I_0}$, thus, ensuring mechanical and electrical coherence on the interfaces.

4.3. Effects of the interface

An interface has a distinct influence on the overall behaviour of a composite. This is usually neglected in classic continuum models which is reasonable for materials where the bulk dominates the behaviour. However, in nanomaterials, interface effects cannot be neglected. Fig. 6 illustrates the role of the interface using a simulation of bulk electromechanical coupling in the sandwich structure first without the interface and then including the purely mechanical behaviour of the interface.

Table 3
Interface material parameters.

	Symbol	Value	Source
Lamé parameters	$\overline{\lambda}$	−2.0 N/**m**	
	$\overline{\mu}$	3.5 N/m	
Electromechanical coupling parameter (electroadsorption)	$\overline{\xi}^{\text{ion}}$	12 J/C	[a]
Electromechanical coupling parameter (interface charge)	$\overline{\xi}^{\text{el}}$	30 J/C	[a]
Diffusivity	$\overline{D}$	$5 \cdot 10^{-8}$ m^2/s	

[a] Provided by N. Mameka at Helmholtz-Zentrum Geesthacht based on Mameka et al. (2014).

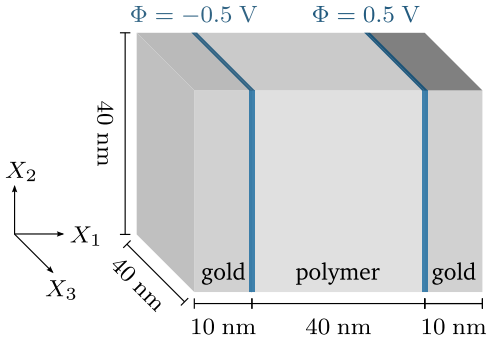

Fig. 5. Sketch of the gold-polymer sandwich structure. The structure's bottom face is rigidly clamped and the potential difference is imposed as a boundary condition on the interface.

It is apparent that by considering the stiffness of the interface, the interface resists the bending imposed by the polymer bulk, yielding a smaller deformation of the gold electrode. As the electric fields depend on the deformation of the composite, there is also a pronounced difference in the ion distribution. Modification of the interface's behaviour, thus, modifies the behaviour of the whole composite.

In Fig. 7, the deformations of the bulk and the interface due to the chemoelectromechanical coupling on the interface and in the bulk polymer illustrates how the interface bends and, depending on the side, contracts or elongates in the X_2 direction. The influence of the chemoelectromechanical coupling on the interface is described further in Section 4.4.

In addition to the mechanical influence, the interface exhibits charge carrier transport. The interface charges arise from electric fields in the bulk which are deformation dependent and, thus, the charge distribution over the interface is not homogeneous. However, as the cahrge carriers diffuse along the interface, ultimately a uniform charge distribution is established, see Fig. 8.

4.4. Effects of electromechanical coupling

Four different mechanisms cause chemoelectromechanical coupling in the metal/ion-conducting polymer composite. In the polymer bulk (Eq. (22)), the coupling arises from differences in ion concentrations and polarisation of the material while on the interface, both interface charges and electroadsorption of ions influence the mechanical response.

The latter two mechanisms are separated in the sandwich setup employed here as it has two differently charged interfaces. For the case of mobile anions, negatively charged anions from the polymer bulk are electroadsorbed onto the “positive” electrode upon which the positive electric potential is applied. The “negative” electrode has a negative interface charge (i.e., a high electron concentration $\bar{c}_0^{\mathrm{el}}$).

Fig. 9 depicts the deformed sandwich structure with chemoelectromechanical coupling activated either in the bulk or on the interface as well as the case in which chemoelectromechanical coupling in the bulk interacts with electromechanical coupling on the interface. Electromechanical coupling in the bulk causes the polymer to swell inregion close to the “positive” electrode where there is an ion excess and to contract in regions of reduced ion concentration, causing a bending deformation of the composite block. For the case of mobile anions as depicted here, the “negative” electrode contracts due to the negative interface charge that strengthens the atomic bonds. In contrast, the “positive” electrode expands upon electroadsorption, resulting in a bending towards the metal electrode. If all three coupling mechanisms are activated, the deformation is increased as both, bulk and interface coupling, act in the same direction.

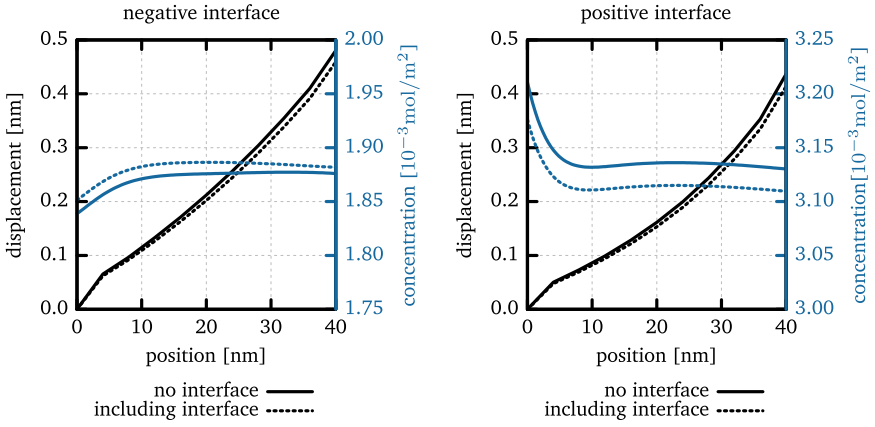

Fig. 6. Difference between the deformation and ion concentration at the interface if interface elasticity is neglected resp. taken into account.

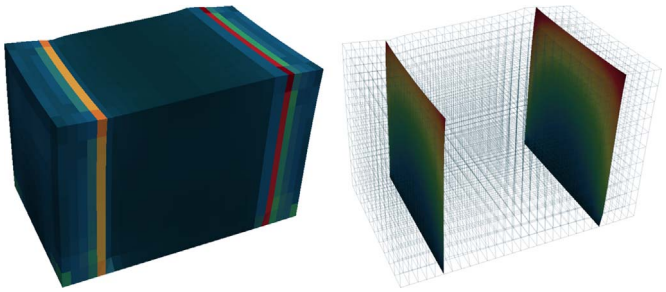

Fig. 7. Plot of deformed bulk and interfaces. The colour map of the bulk specimen illustrates the norm of the stress tensor while for the interface the displacement perpendicular to the interface is shown. Electromechanical coupling on the interface causes curving of the interfaces both along their planes as well as perpendicularly to them.

The electromechanical coupling in the polymer bulk arises due to two different mechanisms as depicted in Fig. 10. Polarisation induces a volumetric expansion of the polymer upon application of a potential difference. By contrast, deformation due to ion migration occurs in regions close to the electrodes in which space charges arise. This type of coupling is responsible for the bending deformation visible in Fig. 9 and is strongly influenced by the superposition of the interface coupling effects which may counteract or amplify the deformation. For the example of a polymer in which only anions are mobile, the interface coupling effects amplify the bulk deformation. However, in many polymer electrolytes, the anion is fixed to the polymer chain and the cation is mobile. This has a significant influence on the actuation behaviour of the composite, as electroadsorption of cation results in a contraction of the interface as opposed to the expansion that arises upon adsorption of anions (Haiss, 2001). This is illustrated Fig. 11, in which the norm of the interface displacement vector $\bar{\boldsymbol{u}}$ is shown over the X_2-length of the interface. As the ion concentration is almost homogeneous along the interface, it deforms evenly upon electroadsorption of either anions or cations. If anions are electroadsorbed onto the interface, the interface expands and curves outwards. The coupling in the bulk polymer acts in the same direction and, thus, amplifies the effect, cf. Fig. 10. If cations are electroasorbed, however, the interface contracts while the polymer close to the interface expands due to increased ion concentration, i.e., interface and bulk coupling are opposing effects, resulting in a more complex deformation behaviour.

5. Summary

A thermodynamically consistent continuum framework for modelling the chemoelectromechanically coupled behaviour of nanoscale metal/ion-conducting polymer composites has been proposed. Due to the nanocomposites' characteristically high interface-to-volume ratio, any modification of the interface strongly affects their mechanical behaviour. Such modification in response to an electric field is fully reversible which makes these nanocomposites excellent candidates for actuation or sensoring applications.

To model the pronounced influence the interface has on the electromechanical response in nanocomposites, the governing equations for deformation, electrostatics and diffusion are developed for the bulk material and on the interface in a general manner. This interface theory is the first to describe a system coupling electromechanical behaviour and diffusive charge carrier transport. This novel framework is then utilised to model the fully coupled behaviour of a nanoporous metal filled with an ion-conducting polymer.

Suitable constitutive equations are formulated that describe different mechanisms of electromechanical coupling in such materials. That is, not only bulk coupling within the ion-conducting polymer but also the modification of the metal/polymer interface through both, the formation of an interface charge and electroadsorption of electrolyte ions, are taken into account. Numerical

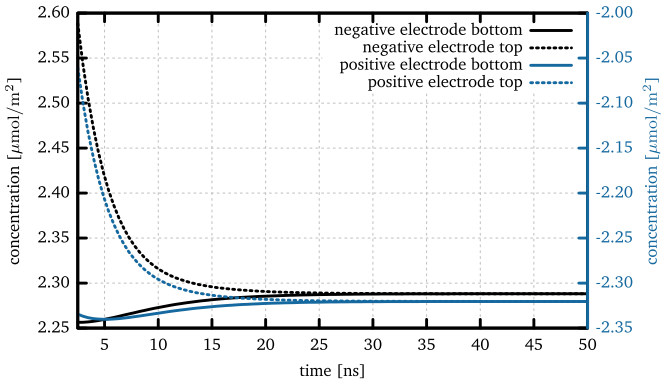

Fig. 8. Variation of the interface electron concentration for two points at the bottom and the top of the specimen for both interfaces. The initial difference due to the deformed geometry is balanced by diffusion along the interface.

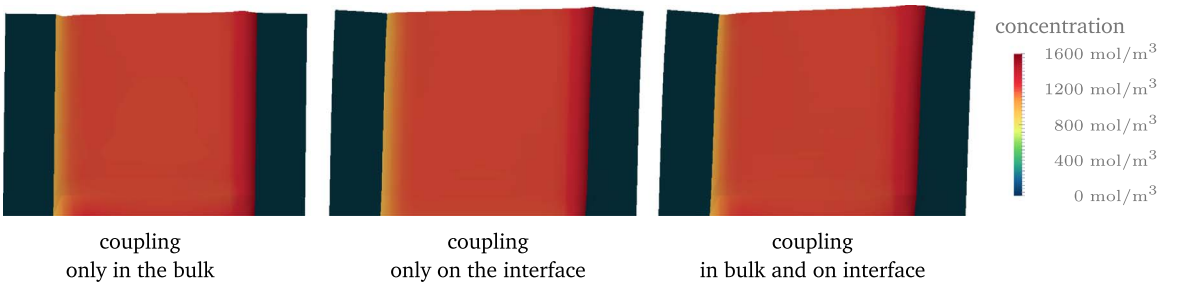

Fig. 9. Comparison of deformation states caused by different electromechanical coupling mechanisms. In the bulk polymer, expansion occurs at the "positive" electrode due to ion excess and contraction arises in regions of reduced ion concentration. If only interface coupling mechanisms are considered, the "negative" electrode contracts due to the interface charge while the "positive" electrode expands upon electroadsorption. These effects are superimposed if the electromechanical coupling in the bulk and on the interface is accounted for.

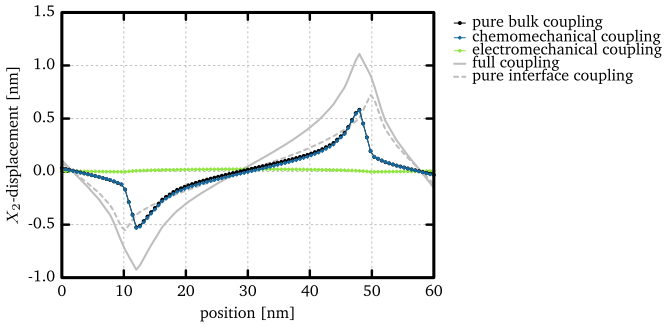

Fig. 10. Displacement at the top of the specimen as induced by different coupling mechanisms. Electromechanically induced deformation caused by polarisation of the material occurs over the whole polymer volume while deformation due to chemomechanical coupling is localised to regions close to the electrodes. The bulk coupling as a superposition of both mechanisms differs only minimally from that induced by chemomechanical coupling.

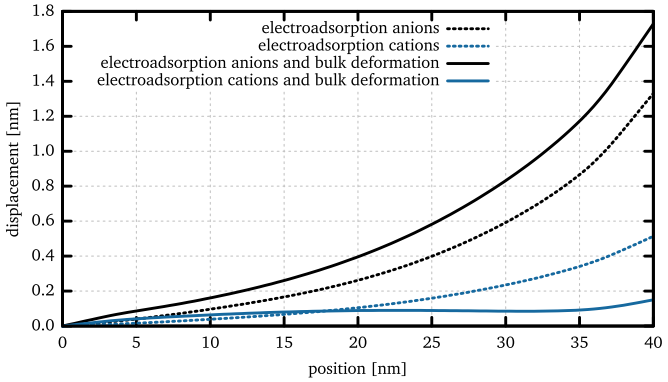

Fig. 11. Norm of interface displacement vector $\bar{u}$ for adsorption of differently charged ions. The deformation due to electroadsorption of anions is amplified by deformation of the bulk polymer, while for the electroadsorption of cations, the effects counteract each other.

studies elucidate the influence of the interface and investigate different coupling mechanisms and their interaction with each other. The results provide valuable insight into the functionality of electroactive nanocomposites.

The framework presented here describes fundamental effects causing actuation in nanoporous metal/polymer composites. Therefore, a natural extension of the model would be the incorporation of sensing behaviour. Furthermore, different factors influencing the electroactive behaviour such as steric effects, capacitive properties and interphase regions should be investigated.

Acknowledgments

We gratefully acknowledge financial support from the German Research Foundation (DFG) (Grant no. SFB 986) via SFB 986 "M^3", project B6. We also thank J. Markmann at Helmholtz-Zentrum Geesthacht (SFB 986, project B2) for very fruitful discussions. Furthermore, we thank the anonymous reviewers for their insightful comments that helped to considerably improve this paper.

Appendix A. Integral energy and entropy balances

The work performed on an electroactive body can be portioned into a mechanical, an electrical and a chemical contribution, see for example Hong et al. (2010) and Nardinocchi et al. (2011) for discussions of the work performed on polyelectrolyte gels and ionic polymers, respectively. Thus, the balance of energy is of the form

$$\dot{\mathcal{E}} = \mathcal{P}^{\text{mechanical}} + \mathcal{P}^{\text{electrical}} + \mathcal{P}^{\text{chemical}}, \tag{40}$$

where $\mathcal{E}$ denotes the system's total energy and $\mathcal{P}$ denotes a power.

In the modelling framework proposed in this contribution, the metal/polymer interface is considered to be energetic, i.e., it has its own energetic behaviour. Hence, contributions for both, the electroactive body $\mathcal{B}_0$ and the interface $\mathcal{I}_0$, are accounted for in the balance equations

$$\dot{\mathcal{E}} = \frac{\mathrm{D}}{\mathrm{D}t}\int_{\mathcal{B}_0}\left[\rho_0\varepsilon + \frac{1}{2}\rho_0\dot{\boldsymbol{u}}\cdot\dot{\boldsymbol{u}}\right]\mathrm{d}V + \frac{\mathrm{D}}{\mathrm{D}t}\int_{\mathcal{I}_0}\left[\overline{\rho}_0\overline{\varepsilon} + \frac{1}{2}\overline{\rho}_0\dot{\overline{\boldsymbol{u}}}\cdot\dot{\overline{\boldsymbol{u}}}\right]\mathrm{d}A. \tag{41}$$

The mechanical power in the volume and on the interface is expressed in terms of the stresses $\boldsymbol{P}$ and $\overline{\boldsymbol{P}}$ and the specific body forces $\boldsymbol{b}$ and $\overline{\boldsymbol{b}}$ according to

$$\mathcal{P}^{\text{mechanical}} = \int_{\partial\mathcal{B}_0}\dot{\boldsymbol{u}}\cdot\boldsymbol{P}\cdot\boldsymbol{N}\,\mathrm{d}A + \int_{\mathcal{B}_0}\rho_0\dot{\boldsymbol{u}}\cdot\boldsymbol{b}\,\mathrm{d}V + \int_{\partial\mathcal{I}_0}\dot{\overline{\boldsymbol{u}}}\cdot\overline{\boldsymbol{P}}\cdot\overline{\boldsymbol{N}}\,\mathrm{d}L + \int_{\mathcal{I}_0}\overline{\rho}_0\dot{\overline{\boldsymbol{u}}}\cdot\overline{\boldsymbol{b}}\,\mathrm{d}A. \tag{42}$$

The electric power in the system arises from changes in the free charge distribution as characterised by the electric displacement field D and external sources of electric energy such as batteries that provide or consume electrons resulting in a change in the electron charge density q_0^{el}:

$$\mathcal{P}^{\text{electrical}} = -\int_{\partial\mathcal{B}_0}\Phi\dot{\mathsf{D}}\cdot\boldsymbol{N}\,\mathrm{d}A + \int_{\mathcal{B}_0}\Phi\dot{q}_0^{\text{el}}\,\mathrm{d}V - \int_{\partial\mathcal{I}_0}\overline{\Phi}\cdot\dot{\overline{\mathsf{D}}}\cdot\overline{\boldsymbol{N}}\,\mathrm{d}L + \int_{\mathcal{I}_0}\overline{\Phi}\dot{\overline{q}}_0^{\text{el}}\,\mathrm{d}A. \tag{43}$$

Furthermore, mass transport within the system contributes to the internal energy of the system, yielding

$$\mathcal{P}^{\text{chemical}} = -\sum_i\int_{\partial\mathcal{B}_0}\varphi^{\text{mix}^i}\boldsymbol{J}^i\cdot\boldsymbol{N}\,\mathrm{d}A + \sum_i\int_{\mathcal{B}_0}\varphi^{\text{mix}^i}W^i\,\mathrm{d}V - \sum_i\int_{\partial\mathcal{I}_0}\overline{\varphi}^{\text{mix}^i}\dot{\overline{\boldsymbol{J}}}^i\cdot\overline{\boldsymbol{N}}\,\mathrm{d}L + \sum_i\int_{\mathcal{I}_0}\overline{\varphi}^{\text{mix}^i}\overline{W}^i\,\mathrm{d}A. \tag{44}$$

The balance of entropy for the isothermal case is

$$\begin{aligned}\frac{\mathrm{D}}{\mathrm{D}t}\left[\int_{\mathcal{B}_0}\rho_0\eta\mathrm{d}V + \int_{\mathcal{I}_0}\overline{\rho}_0\overline{\eta}\,\mathrm{d}A\right] = &-\sum_i\int_{\partial\mathcal{B}_0}\eta^{\text{mix}^i}\boldsymbol{J}^i\cdot\boldsymbol{N}\,\mathrm{d}A + \sum_i\int_{\mathcal{B}_0}\eta^{\text{mix}^i}W^i\,\mathrm{d}V - \sum_i\int_{\partial\mathcal{I}_0}\overline{\eta}^{\text{mix}^i}\overline{\boldsymbol{J}}^i\cdot\boldsymbol{N}\,\mathrm{d}L + \sum_i\int_{\mathcal{I}_0}\overline{\eta}^{\text{mix}^i}\overline{W}^i\,\mathrm{d}A\\ &+\int_{\mathcal{B}_0}\Gamma_0\,\mathrm{d}V + \int_{\mathcal{I}_0}\overline{\Gamma}_0\,\mathrm{d}A.\end{aligned} \tag{45}$$

Here, Γ_0 and $\overline{\Gamma}_0$ denote the entropy production rates in the bulk and on the interface, respectively. Both entropy production terms are non-negative, thus, ensuring that the second law of thermodynamics is obeyed in both domains as well as in the whole system.

Application of the divergence theorems Eqs. (1a) and (1b), localisation and insertion of the governing equations for the deformation, the electrostatic behaviour and the charge carrier transport as summarised in Table 1, finally yield the localised balance Eqs. (16)–(19).

References

Alici, G., Spinks, G.M., Madden, J.D., Wu, Yanzhe, Wallace, G.G., 2008. Response characterization of electroactive polymers as mechanical sensors. IEEE/ASME Trans. Mechatron. 13 (2), 187–196.

Aureli, Matteo, Porfiri, Maurizio, 2013. Nonlinear sensing of ionic polymer metal composites. Contin. Mech. Thermodyn. 25 (2), 273–310.

Aureli, Matteo, Lin, Weiyang, Porfiri, Maurizio, 2009. On the capacitance-boost of ionic polymer metal composites due to electroless plating: theory and experiments. J. Appl. Phys. 105 (10), 104911.

Balk, T.J., Eberl, C., Sun, Y., Hemker, K.J., Gianola, D.S., 2009. Tensile and compressive microspecimen testing of bulk nanoporous gold. JOM 61 (12), 26–31.

Bangerth, W., Hartmann, R., Kanschat, G., 2007. deal.II – a general purpose object oriented finite element library. ACM Trans. Math. Softw. 33 (4), 24/1–24/27.

Bar-Cohen, Y., 2010. 8 – Electroactive polymers as actuators. In: Kenji, Uchino(Ed.). Advanced Piezoelectric Materials. Woodhead Publishing Series in Electronic and Optical Materials,Woodhead Publishing, pp. 287–317.

Borukhov, I., Andelman, D., Orland, H., 2000. Adsorption of large ions from an electrolyte solution: a modified poisson-boltzmann equation. Electrochim. Acta 46 (2–3), 221–229.

Bustamante, R., Rajagopal, K.R., 2013. On a new class of electroelastic bodies. I. Proc. R. Soc. Lond. A: Math. Phys. Eng. Sci. 469 (2149), 1–16.

Cermelli, P., Fried, E., Gurtin, M.E., 2005. Transport relations for surface integrals arising in the formulation of balance laws for evolving fluid interfaces. J. Fluid Mech. 544 (339–351), 12.

Cha, Y., Porfiri, M., 2014. Mechanics and electrochemistry of ionic polymer metal composites. J. Mech. Phys. Solids 71, 156–178.

Cha, Y., Aureli, M., Porfiri, M., 2012. A physics-based model of the electrical impedance of ionic polymer metal composites. J. Appl. Phys. 111 (12), 124901.

Cha, Youngsu, Cellini, Filippo, Porfiri, Maurizio, 2013. Electrical impedance controls mechanical sensing in ionic polymer metal composites. Phys. Rev. E 88 (December), 062603.

Chatzigeorgiou, G., Javili, A., Steinmann, P., 2014. Surface electrostatics: theory and computations. Proc. R. Soc. Lond. A: Math. Phys. Eng. Sci. 470 (2164), 20130628.

Chen, Z., Tan, X., Will, A., Ziel, C., 2007. A dynamic model for ionic polymer-metal composite sensors. Smart Mater. Struct. 16 (4), 1477.

Chi, Z., Xu, Q., 2014. Recent advances in the control of piezoelectric actuators. Int. J. Adv. Robot. Syst. 11, 1–11.

Davydov, D., Voyiatzis, E., Chatzigeorgiou, G., Liu, S., Steinmann, P., Böhm, M.C., Müller-Plathe, F., 2014. Size effects in a silica-polystyrene nanocomposite: molecular dynamics and surface-enhanced continuum approaches. Soft Mater. 12, S142–S151.
Dorfmann, A., Ogden, R.W., 2005. Nonlinear electroelasticity. Acta Mech. 174 (3–4), 167–183.
Dorfmann, A.L., Ogden, R.W., 2014. Nonlinear Theory of Electroelastic and Magnetoelastic Interactions. Springer, US.
Elsner, B.A.M., Müller, S., Bargmann, S., Weissmüller, J., 2017. Surface excess elasticity of gold: Ab initio coefficients and impact on the effective elastic response of nanowires. Acta Mater. 124, 468–477.
Ericksen, J.L., 2007. Theory of elastic dielectrics revisited. Arch. Ration. Mech. Anal. 183 (2), 299–313.
Fang, Y., Tan, X., Shen, Y., Xi, N., Alici, G., 2008. A scalable model for trilayer conjugated polymer actuators and its experimental validation. In: Proceedings from the Advanced Processing of Biomaterials Symposium, Materials Science and Technology Conference and ExhibitionMaterials Science and Engineering: C. vol. 28(3), pp. 421–428.
Farinholt, K., Leo, D.J., 2004. Modeling of electromechanical charge sensing in ionic polymer transducers. Mech. Mater. 36 (5–6), 421–433, (Coupled Chemo-Mechanical Phenomena).
Gurtin, M.E., Murdoch, A.I., 1975. A continuum theory of elastic material surfaces. Arch. Ration. Mech. Anal. 57 (4), 291–323.
Haiss, W., 2001. Surface stress of clean and adsorbate-covered solids. Rep. Prog. Phys. 64 (5), 591.
Hallinan, D.T., Balsara, N.P., 2013. Polymer electrolytes. Annu. Rev. Mater. Res. 43 (1), 503–525.
Hong, W., 2011. Modeling viscoelastic dielectrics. J. Mech. Phys. Solids 59 (3), 637–650.
Hong, W., Zhao, X., Suo, Z., 2010. Large deformation and electrochemistry of polyelectrolyte gels. J. Mech. Phys. Solids 58 (4), 558–577.
Javili, A., Steinmann, P., 2010. On thermomechanical solids with boundary structures. Int. J. Solids Struct. 47 (24), 3245–3253.
Javili, A., McBride, A., Steinmann, P., 2013. Thermomechanics of solids with lower-dimensional energetics: on the importance of surface, interface, and curve structures at the nanoscale. A unifying review. Appl. Mech. Rev. 65, (010802-010802-31).
Javili, A., McBride, A., Steinmann, P., Reddy, B.D., 2014. A unified computational framework for bulk and surface elasticity theory: a curvilinear-coordinate-based finite element methodology. Comput. Mech. 54 (3), 745–762.
Jin, H.-J., Weissmüller, J., 2010. Bulk nanoporous metal for actuation. Adv. Eng. Mater. 12 (8), 714–723.
Jo, C., Pugal, D., Oh, I.-K., Kim, K.J., Asaka, K., 2013. Recent advances in ionic polymer-metal composite actuators and their modeling and applications. Prog. Polym. Sci. 38 (7), 1037–1066.
Kilic, M.S., Bazant, M.Z., Ajdari, A., 2007. Steric effects in the dynamics of electrolytes at large applied voltages. ii. Modified poisson-nernst-planck equations. Phys. Rev. E 75, 021503.
Lang, X., Zhang, L., Fujita, T., Ding, Y., Chen, M., 2012. Three-dimensional bicontinuous nanoporous au/polyaniline hybrid films for high-performance electrochemical supercapacitors. J. Power Sources 197, 325–329.
Laser, D.J., Santiago, J.G., 2004. A review of micropumps. J. Micromech. Microeng. 14 (6), R35.
Lòpez Cascales, J.J., Otero, T.F., 2004. Molecular dynamic simulation of the hydration and diffusion of chloride ions from bulk water to polypyrrole matrix. J. Chem. Phys. 120 (4), 1951–1957.
Mameka, N., Markmann, J., Jin, H.-J., Weissmüller, J., 2014. Electrical stiffness modulation-confirming the impact of surface excess elasticity on the mechanics of nanomaterials. Acta Mater. 76 (0), 272–280.
Mazzoldi, A., Degl'Innocenti, C., Michelucci, M., De Rossi, D., 1998. Actuative properties of polyaniline fibers under electrochemical stimulation. Mater. Sci. Eng.: C 6 (1), 65–72.
McBride, A.T., Javili, A., Steinmann, P., Bargmann, S., 2011. Geometrically nonlinear continuum thermomechanics with surface energies coupled to diffusion. J. Mech. Phys. Solids 59 (10), 2116–2133.
McBride, A., Mergheim, J., Javili, A., Steinmann, P., Bargmann, S., 2012. Computational micro-to-macro transitions for heterogeneous material layers accounting for in-plane stretch. J. Mech. Phys. Solids 60 (6), 1221–1239.
McBride, A., Javili, A., Steinmann, P., Reddy, B.D., 2015. A Finite Element Implementation of Surface Elasticity at Finite Strains Using the Deal.ii library. arXiv:1506.01361.
McEvoy, M.A., Correll, N., 2015. Materials that couple sensing, actuation, computation, and communication. Science 347 (6228).
Mutlu, R., Alici, G., Xiang, X., Li, W., 2014. Electro-mechanical modelling and identification of electroactive polymer actuators as smart robotic manipulators. Mechatronics 24 (3), 241–251, (ISSN 0957-4158).
Nardinocchi, P., Pezzulla, M., Placidi, L., 2011. Thermodynamically based multiphysic modeling of ionic polymer metal composites. J. Intell. Mater. Syst. Struct. 22 (16), 1887–1897.
Nemat-Nasser, S., Li, J.Y., 2000. Electromechanical response of ionic polymer-metal composites. J. Appl. Phys. 87 (7), 3321–3331.
Porfiri, M., 2008. Charge dynamics in ionic polymer metal composites. J. Appl. Phys. 104 (10), 104915.
Pugal, D., Kim, K.J., Aabloo, A., 2011. An explicit physics-based model of ionic polymer-metal composite actuators. J. Appl. Phys. 110 (8), 084904.
Pugal, D., Solin, P., Kim, K.J., Aabloo, A., 2012. Modeling ionic polymer-metal composites with space-time adaptive multimesh hp-fem. Commun. Comput. Phys. 11 (1), 249–270.
Schicker, D., Wallmersperger, T., 2013. Modeling and simulation of the chemo-electro-mechanical behavior of ionic polymer-metal composites. J. Appl. Phys. 114 (16), 163709.
Shahinpoor, M., Bar-Cohen, Y., Simpson, J.O., Smith, J., 1998. Ionic polymer-metal composites (IPMCs) as biomimetic sensors, actuators and artificial muscles - a review. Smart Mater. Struct. 7 (6), R15.
Uchino, K., 2010. 1 – The development of piezoelectric materials and the new perspective. In: Uchino, Kenji(Ed.). Advanced Piezoelectric Materials, Woodhead Publishing Series in Electronic and Optical Materials, Woodhead Publishing. pp. 1–85.
Vernitskaya, T.V., Efimov, O.N., 1997. Polypyrrole: a conducting polymer; its synthesis, properties and applications. Russ. Chem. Rev. 66 (5), 443.
Wang, K., Weissmüller, J., 2013. Composites of nanoporous gold and polymer. Adv. Mater. 25 (9), 1280–1284.
Weissmüller, J., Viswanath, R.N., Kramer, D., Zimmer, P., Würschum, R., Gleiter, H., 2003. Charge-induced reversible strain in a metal. Science 300 (5617), 312–315.
Wilson, S.A., Jourdain, R.P.J., Zhang, Q., Dorey, R.A., Bowen, C.R., Willander, M., Ul Wahab, Q., Willander, M., Al-hilli, S.M., Nur, O., Quandt, E., Johansson, C., Pagounis, E., Kohl, M., Matovic, J., Samel, B., van der Wijngaart, W., Jager, E.W.H., Carlsson, D., Djinovic, Z., Wegener, M., Moldovan, C., Iosub, R., Abad, E., Wendlandt, M., Rusu, C., Persson, K., 2007. New materials for micro-scale sensors and actuators: an engineering review. Mater. Sci. Eng.: R: Rep. 56, 1–129.